HYDROMECHANICAL BEHAVIOR OF SANDS UNDER PROPORTIONAL TRIAXIAL COMPRESSION TESTS

Van Hung Nguyen[1;2], Jean Guélard[1], Nicolas Gland[1], Jérémie Dautriat[1], Christian David[2]
[1] IFP Energies nouvelles, 1&4 Av. de Bois Préau, 92852 Rueil-Malmaison Cedex, France
[2] U.C.P., Lab. Géosciences & Environnement, 5 mail Gay Lussac, 95031 Cergy, France.

This paper was prepared for presentation at the International Symposium of the Society of Core Analysts held in Austin, Texas, USA 18-21 September, 2011

ABSTRACT

Performance of reservoirs and wells in unconsolidated formations involve many challenges from hydromechanical properties viewpoint. The large deformation of these unconsolidated reservoirs during production, mainly induced by fluid pressure changes, have an important impact on the performance of the wells but also lead to strong modification of the flow properties at the scale of the whole reservoir. Coupled mechanical and transport studies on such weakly cohesive reservoir rocks, difficult and too rare, are needed to understand the interaction between fluid pressure, deformation and performance of these reservoirs. Classically the mechanical loadings applied in the laboratory are hydrostatic or deviatoric at constant confining pressure; however the in-situ stress-paths experienced by the reservoirs differ due to complex geology. We need thus to perform loading tests with more appropriate conditions such as proportional triaxial with different stress path parameters K where K refers to the ratio of change in confining pressure to change in axial stress. We use a triaxial flow cell to perform proportional triaxial compression tests under stress path ratio $0<K<1$ in drained conditions and permeability measurements on quartz sands in order to determine both their hydromechanical (permeability and compressibilities) and elastoplastic properties. For all tests, the porosity and permeability reductions depend on the stress-path coefficient, the grain angularity and the granular packing. Observations are rationalised through consideration of plastic yielding controlled by elliptical caps. The magnitude of compactive yield stresses increases with roundness of the particles at fixed size (~1mm). The samples are damaged either in the 1-30 *MPa* or 1-60 *MPa* pressure ranges depending on the magnitude of the hydrostatic yield stress; on the basis of compressibilities and permeability evolutions, for the studied rounded particles the critical pressure at failure is 30 *MPa* whereas for the sharp sands, the critical pressure is around 10 *MPa*. For sharp grains, the yield stresses, difficult to identify on the stress-strain curves characterized by smooth evolutions, are obtained by the maximum curvature criterion; this results from a progressive damage of the grains by the abrasion of the angular edges. Grain damage is analysed by Laser Diffraction Particle Size Analyser. Permeability reductions can reach 10% with the elastic deformation and drop down by two orders of magnitude in the plastic deformation regime.

EXPERIMENTAL METHODOLOGY

The triaxial flow cell (ErgoTech Ltd) used in this study is described in Dautriat et al., [1]. Temperature is regulated at 40°*C*. The axial, confining and pore pressures can be controlled independently up to 10 *kPsi* (~69 *MPa*). In proportional testing, the stress path parameter *K* refers to the ratio of change in confining pressure to change in axial stress $K = \Delta\sigma_r / \Delta\sigma_a$ and is bounded between *K*=0 (conventional triaxial compression test at constant confining pressure) and *K*=1 (hydrostatic compression test). Such a methodology adopted by many authors [2,3,4] gives the possibility of investigating stress states for complex reservoir structures which require more than a simple uniaxial strain assumption. Axial piston displacement is measured by external LVDT and radial deformation of cores is measured by a cantilever type extensometer. Compaction-driven pore volume change (pressurized drained fluid) is measured by a capacitive level sensor. For drained compression tests, pore fluid was 20g/L NaCl brine at a pressure of 1 *MPa*. For permeability tests, viscous oil (marcol 172, 26cp@40°C) was used to provide sufficient measurable pressure drop. The differential of pressure is measured using local fluid pressure sampling ports molded in the elastomer sleeve and located at 1cm of each core ends (avoiding system pressure drop). High permeability sands were measured using steady-state multi-steps or continuous flow during compaction. Here, only standard vertical (axial) permeability measurements are presented; later on we plan to complete our data set with horizontal (radial) permeability measurements to reproduce lateral flow in a reservoir. Glass spheres and Quartz Durance sand were selected for testing respectively as analogue of rounded and angular sands with narrow particle size distribution centered close to 1mm after seeving in the range 1-1.1mm. The grain size distribution was characterized by Laser Diffraction apparatus (Horiba): small differences between the particle size distributions of glass spheres and sand were observed due to differences in the shape and angularity of the particles. Compacted samples are prepared directly in the sleeve of diameter 38.1mm in the cell. After tapping protocol, the porosity is estimated around ϕ=37±1% for glass beads and about ϕ=40%±1% for Durance sand.

RESULTS AND DISCUSSION

Figure 1 shows the concomitant evolution of axial deformation (a) and permeability (b) with applied stress on triaxially compacted glass beads. Figure 2 shows corresponding results obtained on Durance Sand; all tests were started at 3 *MPa* confining pressure. The onset of plastic collapse (initiation of pervasive grain crushing) under isotropic loading conditions (*K*=1.0) is observed (Figure 1a) to occur sharply at *P**~30 *MPa*, picked as the endpoint of the elastic of deformation regime. P^* may also be estimated by the diagram and power law $P^* \propto (\phi R)^{-n}$ proposed by Zhang et al., [5] on the basis of Hertzian contact theory and crack propagation mechanics where ϕ is porosity, *R* is the grain radius and *n*=3/2; this power law relation has been tested by Wong et al., [6] on porous sandstones and glass spheres and Karner et al., [7] on rounded quartz sand. The estimated value using this model on the glass spheres is around 30 *MPa*, in good agreement with the measured value. For the Durance sand there is no such abrupt onset on the curvature in the stress-strain curve. To identify the yield stress the point of maximum curvature has

been detected; the mean stress yield point is P^*~10 *MPa* smaller than the estimation P^*~20 *MPa* obtained by Zhang et al. formula [5]. For both glass beads and sand, the permeability evolutions show two regimes: one corresponding to the elastic deformation of the granular packing associated with small reduction of the pore and throat sizes, and the other one corresponding to non-reversible damage of the grains associated with strong modification of the pore space characterized with much smaller pores and a bigger tortuosity. For Durance Sand, the transition between both regimes is less pronounced as the damage process responsible for the second regime seems to be more continuous. Post-test Particle Laser Diffraction of samples deformed under K=1 stress paths (Figure 3(a) and Figure 3(b)) show that grain damage (peak collapse and tail of distribution down to 100µm) has indeed occurred for the two materials. Therefore, it appears that this formula applies for rounded particles but not for angular ones. The measurements of permeability under stress show the existence of a boundary separating two regions: one where the permeability seems only slightly changed and the other one where the permeability decreases sharply from the initial permeability by one to two orders of magnitude. Figure 4(a) and Figure 4(b) show volumetric deformation results obtained on triaxial compacted Durance Sand respectively in *Dry* and *Drained* (brine saturated) conditions. *Dry* tests were started close to 0.1 *MPa* while *Drained* tests were started slightly below 1 *MPa* for sealing. Our results in the low pressure range (<1 MPa) might be influenced by sleeve conformance. Dry sand appears to be stiffer than saturated sand, bulk modulus being 1/3 higher in dry condition (0.35 *GPa* compared to 0.23 *GPa*). This is due to a friction weakening effect at grains contacts in presence of water. In the *Drained* experiment, both volumetric strains measurements (obtained from combined LVDT and radial extensometer -not showed- and from pore volume change) match well for all stress paths K except for the lowest K=0.2; pore volume change exhibit monotonous compaction while bulk measurement from radial extensometer shows a final dilatancy; barrel shape geometric evolution of samples at high deviatoric stress may lead to incorrect volume interpretation. Particle Laser Diffraction of compressed samples (Figure 3(b)) show that grain damage degree increases at lower stress path where deviatoric stress and shear strain are higher. Following Wong et al. notation [6], yield stresses C^* (for stress path $0 \le K < 1$) and P^* (for loading hydrostatic K=1) were identified for all stress paths on volumetric strain ε_v – mean stress P curves in *Dry* condition in Figure 4 and reported on normalized mean stress P – deviatoric stress Q diagram in Figure 5(b). Yield Stresses values in *Drained* conditions are close except for K=0.6.

In general, four constituents are required for full description of elastoplastic material response, which can be obtained from experimental observations [8]: elastic properties yield surface, plastic potential and hardening parameter. Laboratory stress path testing serves to map out combinations of yield surface shape for a particular geomaterial. Changes of stress remaining inside the current yield surface corresponds essentially to recoverable deformation (region of elastically attainable combinations of effective stress). The “modified Cam-clay” elastoplastic model [8] consists in a yield function defining this boundary as $f(P', Q, P^*) = Q^2 + M^2 P'(P' - P^*)$ with the parameter M controlling its elliptic shape and P^* controlling its size. From experiments on various sandstones, Wong

et al., [6] have proposed the normalized yield surface $((P/P^* - \gamma)^2/(1-\gamma)^2) + ((Q+P)^2/\gamma^2) = 1$. For the modified Cam-Clay Model, best fits give (M=0.85; P^*=30 *MPa*) for glass beads and (M=1.1; P^*=10 *MPa*) for Durance sand (Figure 5). The results for Durance sand are also compatible with Wong et al. [6] model (P^*=10 *MPa*, γ=0.5, δ=0.55) as shown in Figure 5(b). After determining the initial yield cap of Durance Sands, additional triaxial compression tests were performed (Figure 6(a)) following composite stress paths (A-B-C) designed to mimic in laboratory a "maximum initial effective stress after burial" (consolidation pressure P_{co}) prior to triaxial loadings (C-D). The insert in Figure 6(a) is a zoom of the curves after the preconsolidation step. Stress-strain curves with K<1 have been slightly shifted to match the starting point of the K=1 curve, in order to better detect the yield stresses. In order to assess the applicability of the elastoplastic model for the Durance Sand, we calculated the elastic moduli, the "swelling coefficient" κ and the "compressibility coefficient" λ. On Figure 6(b), we compare the experimental data and the modeling. Then, following Crawford et al. [4] we model the permeability as $k = k_0.\exp(C.\varepsilon_{eff})$, where k_0 is the initial permeability, C is a material constant and $\varepsilon_{eff} = \sqrt{\varepsilon_{vol}^2 + \varepsilon_{dev}^2}$. For stress path K=1, C=14 allows to reproduce well the permeability evolution of Figure 2(b).

CONCLUSIONS

As most of world's oil and gas wells are drilled in siliciclastic reservoirs and many new discoveries are made in unconsolidated sands or weakly cemented sandstones, understanding soft rock behavior sufficiently to predict reservoir performance and anticipate damage and failure require experimental characterization coupling petrophysics and geomechanics as well as elastoplatic modelling issues. Their hydromechanical behaviour is complex and depends on the stress-path coefficient [2], the grain sharpness and the granular texture [9]. First we performed proportional triaxial compression tests on simple analogue material consisting in compacted glass spheres, to test existing models. Then we tested a more representative natural material, the Durance sand. We identified the yield stresses using the point of maximum curvature of strain-stress curves. While the hydrostatic yield stress P^* of rounded particles is compatible with the powerlaw proposed by Zhang et al. [5], the model overestimates the critical pressure in the case of sands made of angular particles. Modified Cam-Clay and Wong et al's Yield Cap models can capture the onset of plasticity observed in unconsolidated sands. Analysis of particle size distribution highlights the role of shear stress on the degree of particle damage, in agreement with the higher permeability reduction with shear stress and strain. Using constitutive modelling to derive elastoplastic material properties and Crawford et al's equation, an attempt was made to reproduce the evolution of permeability of Durance sand (K=1.0) based on measured and fitted volumetric and shear strains. Additional work is in progress to integrate all the data.

ACKNOWLEDGEMENTS

We thank Sibelco Group for providing the sand, both reviewers for their constructive comments and IFPEN for permission to publish this study.

REFERENCES

1. Dautriat, J., Gland, N., Youssef, S., Rosenberg, E., and Bekri, S., "Stress-dependent directional permeabilities of two analog reservoir rocks: a prospective study on contribution of µ-tomography and pore network models", *SPE Res. Eval. & Eng*., (2009) **12**, 2, 297-310.
2. Crawford, B.R., Gooch, M.J., and Webb, D.W., Textural controls on constitutive behavior in unconsolidated sands: Micromechanics and cap plasticity, *Proc. North America Rock Mech. Symp*., (2004), Houston, TX, USA.
3. Brignoli, M., and Di Federico, A., Compaction of unconsolidated sands and stress path effects: Laboratory evidence, *Proc. North America Rock Mech. Symp.,* (2004), Houston, TX, USA.
4. Crawford, B.R., Webb, D.W., Searles, K.H., Plastic compaction and anisotropic permeability development in Unconsolidated Sands, *Proc. US Rock Mech. Symp*., (2008), S.F., CA,USA.
5. Zhang, J., Wong, T.-F., and Davis, D. M., "Micromechanics of pressure induced grain crushing in porous rocks", *J. Geophys. Res.*, (1990) **95**, B1, 341-352.
6. Wong, T.-F., David, C., and Zhu W**.,** "The transition from brittle faulting to cataclastic flow in porous sandstones: Mechanical deformation", *J.Geophys. Res.*, (1997) **102**, B2, 3009-3025.
7. Karner, S.L., Chester, J.S., Chester, F.M., Kronenberg, A.K., and Hajash, Jr. A., "Laboratory deformation of granular quartz sand: Implications for the burial of clastic rocks", *AAPG Bull.*, (2005) **89**, 5, 603-625.
8. Wood, D.M., *Soil behaviour and critical state soil mechanics*, Cambridge U. P., (1990), 462pp.
9. Mesri, G., and Vardhanabhuti, B**.**, "Compression of granular materials", *Can. Geotech. J*., (2009) **46**, 4, 369-392.

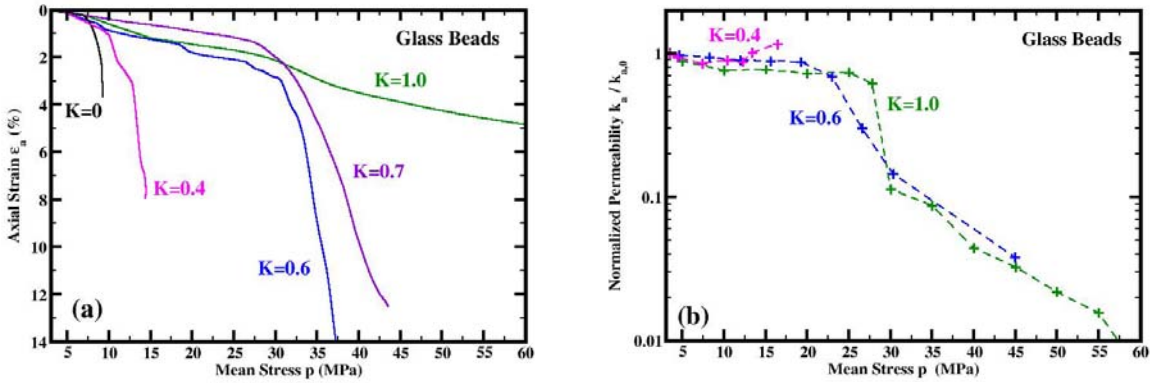

Figure 1: Stress path dependent (a) axial strain evolutions and (b) axial permeability to oil (step measurements) evolutions for Glass Beads. Measurements are affected by damage and creep.

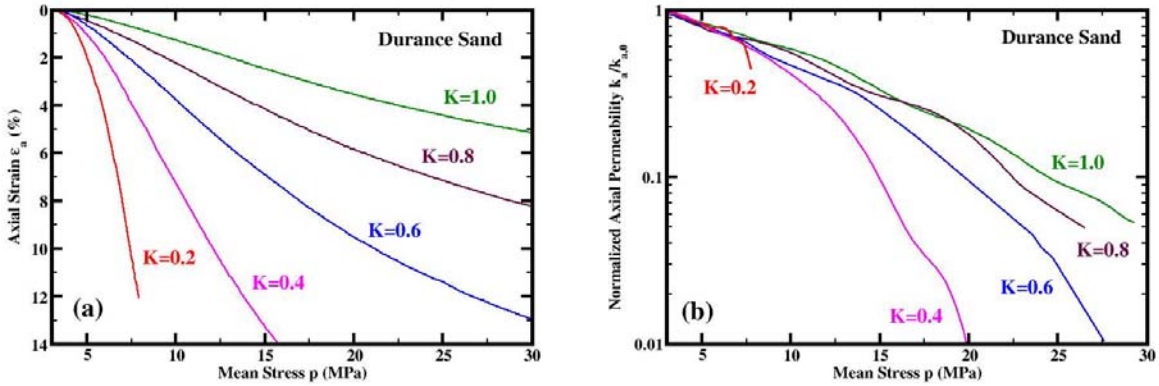

Figure 2: Stress path dependent (a) axial strain evolutions and (b) axial permeability to oil (continuous measurements) evolutions for Durance Sand.

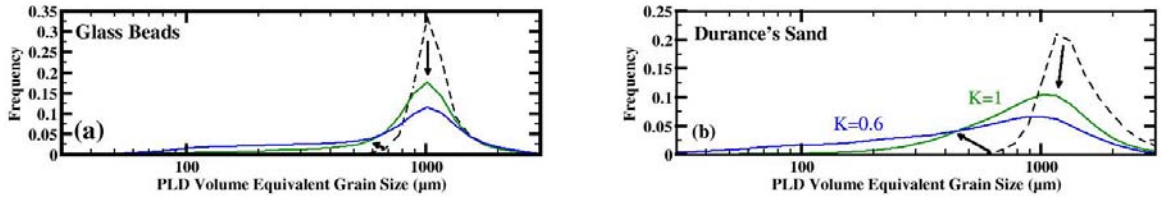

Figure 3: Damage characterization of grain by Particle Lazer Diffraction: (a) for Glass Beads and (b) for durance Sand.

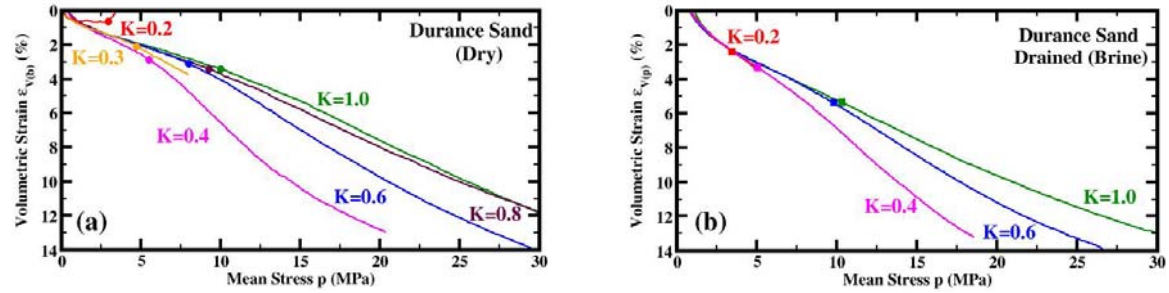

Figure 4: Stress path dependent volumetric strains evolutions in (a) dry state (from bulk deformation) and (b) brine drained state (from pore deformation) for Durance Sand.

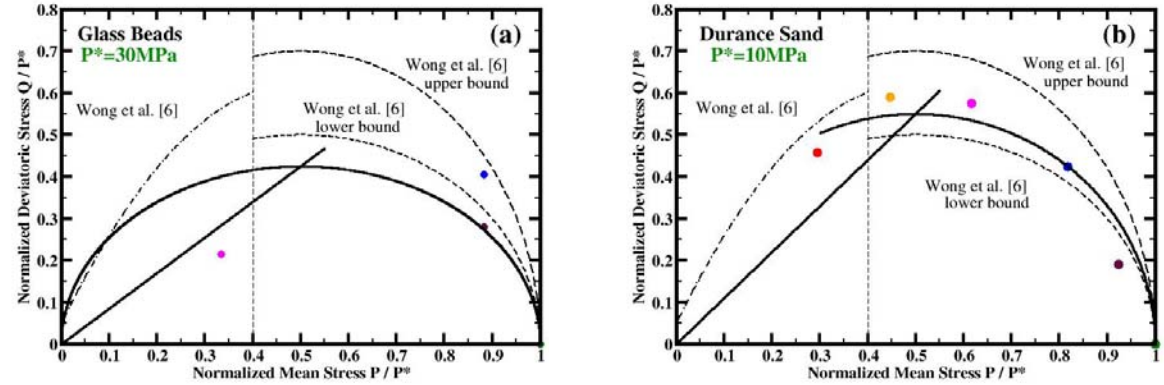

Figure 5: Normalized Yield Caps to P* for (a) Glass Beads (Modified Cam-Clay) and (b) Durance Sand (compatible with Wong et al. [6] bounds defined on porous rocks).

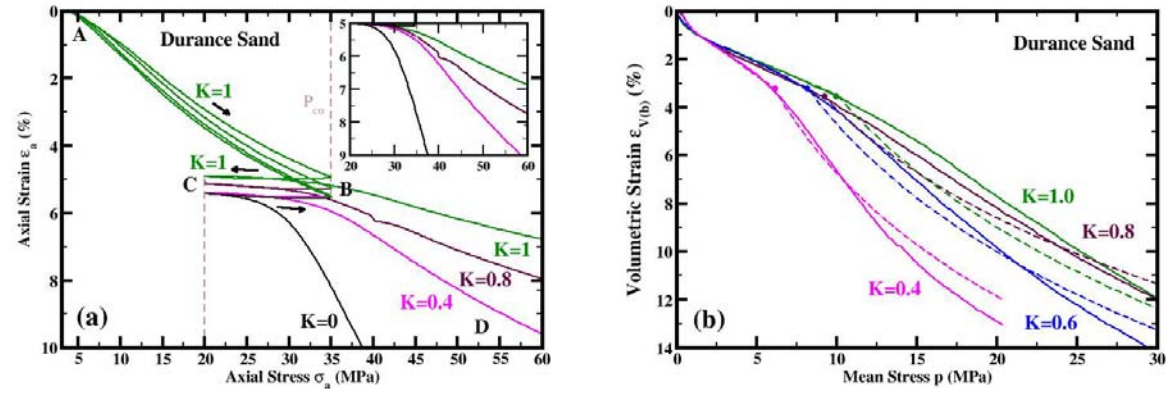

Figure 6: (a) Stress path dependent axial strains evolutions after preconsolidation cycle for Durance Sand and zoom on the curves (triaxial compression steps C-D) after shifting on the *K*=1 preconsolidation cycle (hydrostatic path A-B-C); (b) Model of stress-path dependent strains using Elastoplastic formalism.